Charge carrier recombination dynamics in perovskite and polymer solar cells

Andreas Paulke, Samuel D. Stranks, Juliane Kniepert, Jona Kurpiers, Christian M. Wolff, Natalie Schön, Henry J. Snaith, Thomas J. K. Brenner, and Dieter Neher

---

Articles you may be interested in

Free carrier generation and recombination in PbS quantum dot solar cells
Appl. Phys. Lett. **108**, 103102 (2016); 10.1063/1.4943379

Relation between charge carrier density and lifetime in polymer-fullerene solar cells
J. Appl. Phys. **112**, 044502 (2012); 10.1063/1.4746787

Charge carrier concentration and temperature dependent recombination in polymer-fullerene solar cells
Appl. Phys. Lett. **95**, 052104 (2009); 10.1063/1.3202389

Bimolecular recombination in polymer/fullerene bulk heterojunction solar cells
Appl. Phys. Lett. **88**, 052104 (2006); 10.1063/1.2170424

Double injection as a technique to study charge carrier transport and recombination in bulk-heterojunction solar cells
Appl. Phys. Lett. **87**, 222110 (2005); 10.1063/1.2137454

Charge carrier recombination dynamics in perovskite and polymer solar cells

Andreas Paulke,[1] Samuel D. Stranks,[2,3,4] Juliane Kniepert,[1] Jona Kurpiers,[1] Christian M. Wolff,[1] Natalie Schön,[1] Henry J. Snaith,[2] Thomas J. K. Brenner,[1] and Dieter Neher[1]

[1]Institute of Physics and Astronomy, University of Potsdam, Karl-Liebknecht-Str. 24–25, 14476, Potsdam, Germany
[2]Clarendon Laboratory, Department of Physics, University of Oxford, Parks Road, Oxford OX1 3PU, United Kingdom
[3]Research Laboratory of Electronics, Massachusetts Institute of Technology, 77 Massachusetts Avenue, Cambridge, Massachusetts 02139, USA
[4]Cavendish Laboratory, JJ Thomson Avenue, Cambridge CB3 0HE, United Kingdom

Time-delayed collection field experiments are applied to planar organometal halide perovskite ($CH_3NH_3PbI_3$) based solar cells to investigate charge carrier recombination in a fully working solar cell at the nanosecond to microsecond time scale. Recombination of mobile (extractable) charges is shown to follow second-order recombination dynamics for all fluences and time scales tested. Most importantly, the bimolecular recombination coefficient is found to be time-dependent, with an initial value of ca. 10^{-9} cm^3/s and a progressive reduction within the first tens of nanoseconds. Comparison to the prototypical organic bulk heterojunction device PTB7:PC$_{71}$BM yields important differences with regard to the mechanism and time scale of free carrier recombination. © 2016 AIP Publishing LLC. [http://dx.doi.org/10.1063/1.4944044]

The performance of hybrid perovskite solar cells has improved remarkably in a very short period of time, with power conversion efficiencies already exceeding 20%.[1] While early devices had a structure similar to that of dye sensitized solar cells, with the perovskite layer sandwiched between a mesoporous TiO_2 scaffold and an organic hole-transport layer,[2] the more recently developed planar device architecture places the perovskite layer between two organic planar charge extraction layers,[3] thus resembling the design of multilayer organic solar cells.[4]

In case of efficient (and field-independent) free charge generation, the photovoltaic device performance is determined by the competition between the recombination of free charges and extraction.[5,6] For organic solar cells, there is abundant experimental evidence that charge recombination proceeds via a second order non-Langevin process.[7] Recombination data at low fluences are widely explained with a time-independent bimolecular recombination coefficient k_2. Values for k_2 range typically between 10^{-12} and 10^{-11} cm^3/s depending on the material and preparation condition. Interestingly, second order recombination has been proven to dominate the photocurrent loss for a very wide range of active layer morphologies and materials, including polymers and small molecules.

For perovskite-based cells, despite the rapid progress, less is known about the mechanism of how photogenerated charges recombine, especially in relation to film morphology and the interfaces between the perovskite and the charge transport layers (see the recent paper by Sum *et al.*[8] for the state of the art knowledge).

For neat layers of $CH_3NH_3PbI_3$ (MAPbI$_3$) and the mixed halide perovskite $CH_3NH_3PbI_{3-x}Cl_x$ (MAPbI$_{3-x}$Cl$_x$), in the absence of additional charge extraction layers, the intrinsic charge carrier dynamics were intensively studied with time-resolved

contactless-methods, such as time-resolved photoluminescence[9,10] (TRPL), transient absorption (TAS),[11] optical-pump terahertz-probe spectroscopy,[12] and time-resolved microwave conductivity (TRMC) experiments.[13] The results of time- and fluence-dependent measurements were generally explained by the combination of first order (trap-assisted), second order (free carrier), and third order (Auger-type) recombination processes, with time-independent recombination coefficients. An overview of studied materials and the obtained coefficients with the corresponding references can be found in the supplementary material,[14] with bimolecular recombination coefficients, ranging between 10^{-10} and 10^{-9} cm^3 s^{-1}. The rather small spread of the published values is rather surprising given the large variation of active layer morphologies and efficiencies. With mobilities up to 10 cm^2/Vs, this corresponds to a reduction of the Langevin type recombination rate by approximately five orders of magnitude. Accordingly, long free carrier lifetimes of several hundreds of nanoseconds and free carrier diffusion lengths exceeding $1\,\mu$m have been recorded in in MAPbI$_3$-based materials.[12,15–17]

Transient experiments including charge extraction layers are quite rare, but consistently and repeatedly revealed a rapid depopulation of the free carrier density in the perovskite layer when a suitable hole- or electron-transporting layer was deposited on top.[15,16,18,19] This was explained by the high diffusion coefficients in combination with long free carrier lifetimes. Depending on the composition and thickness of the perovskite layer and the nature of the charge-transporting molecules, charge extraction times range between few hundreds of picoseconds and several nanoseconds.[15,16,19]

Here, we compare the recombination behavior of a planar hybrid perovskite solar cell and an efficient organic bulk heterojunction device, using the method of time-delayed
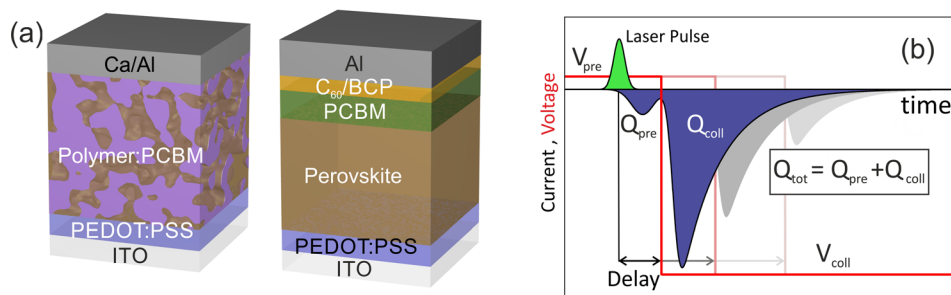
FIG. 1. (a) Schematic device structures of the investigated organic bulk hetero-junction and planar perovskite devices (from left to right) and (b) schematic of the time-delayed collection field (TDCF) experiment.

collection field (TDCF). Despite the fact that perovskite photovoltaic devices are conceptually similar to organic devices, we find that there are fundamental differences in the recombination processes. We also present a versatile approach to analyze TDCF recombination data with regard to the time- and fluence-dependence of free charge recombination.

The TDCF technique is a powerful method to probe the charge carrier dynamics in fully functional solar cells at charge densities which are similar to those obtained under full sunlight illumination conditions. A schematic of the working principle is shown in Figure 1(b). Most importantly, TDCF is an optical pump – electrical probe method and, therefore, sensitive to the fate of extractible charge. In a TDCF experiment, charge carriers are photogenerated by a short (nanosecond) laser pulse, while the device is held at a variable operating voltage (pre-bias V_{pre}), e.g., at the maximum power point or near V_{oc}. The charge carriers are subsequently extracted by a strong reverse bias (collection bias V_{coll}), with a variable delay with respect to the laser pulse. A longer delay allows recombination to evolve for a well-defined time. The analysis of the extracted charge (Q_{pre}) during pre-bias and the extracted charge (Q_{coll}) during application of the collection bias yields dynamic information on how charges move and recombine in the photovoltaic device.[20–22]

The schematic device structures of the two devices studied here are shown in Figure 1(a). The all-organic device consists of a ca. 100 nm thick bulk heterojunction blend of poly[[4,8-bis[(2-ethylhexyl)oxy]benzo[1,2-b:4,5-b′]dithiophene-2,6-diyl][3-fluoro-2-[(2-ethylhexyl)carbonyl]thieno[3,4-b]thiophenediyl]] (PTB7) with [6,6]-phenyl-C71-butyric acid (PC$_{71}$BM). This material combination is known for its high performance in single junction organic solar cells,[23] with power conversion efficiencies of up to 9%. In the planar perovskite device, a ca. 300 nm thick layer of $CH_3NH_3PbI_3$ is sandwiched between a planar film of poly(3,4-ethylenedioxythiophene) polystyrene sulfonate (PEDOT:PSS) and [6,6]-phenyl-C61-butyric acid (PC$_{61}$BM), the latter serving as the electron-selective extraction layer.[3] Though the efficiencies of the studied devices are below those of record cells published in the literature, they all exhibit reasonably high fill factors and short circuit currents (the full set of device parameters is listed in the supplementary material). Notably, these devices have approximately equal comparable power conversion efficiencies, allowing for an easy comparison of the results among these cells. Also, both types of devices exhibited negligible current-voltage hysteresis effects, which is an important prerequisite for the study of the charge recombination mechanism under an applied bias. Details on device

fabrication of each type of solar cell can be found in the methods section of the supplementary material.

Recombination dynamics of PTB7:PCBM organic bulk heterojunction solar cells have been extensively studied.[24,25] Given the similar architecture and power conversion efficiency, this device serves as a proper reference for the planar perovskite device discussed below. Kniepert *et al.* combined time-delayed collection field experiments with steady state JV-measurements and -simulations to investigate nongeminate recombination under working conditions.[22] The results could be conclusively explained on the basis of second-order free carrier recombination, with a time-independent bimolecular recombination coefficient. Figure 2(a) depicts the results of TDCF measurements on a different batch as in Ref. 22 for pulse fluences between 0.2 $\mu J/cm^2$ and 0.6 $\mu J/cm^2$. Excitation was at 500 nm with a pulse length of 5 ns. The data, plotted on a logarithmic time scale as a function of delay time t_d, display the typical features reported earlier for other organic solar cells.[26] Increasing t_d results in a continuous increase of Q_{pre}, as more and more charges leave the device prior to application of the collection pulse. On the other hand, Q_{coll}, the charge present in the layer at time t_d, drops continuously towards zero, as charge becomes either extracted or recombines non-geminately. Also plotted is the total charge $Q_{tot} = Q_{pre} + Q_{coll}$, which is the initially photogenerated charge reduced by all recombination losses during delay. Similar to Q_{coll}, Q_{tot} exhibits a continuous drop with increasing t_d and saturates at a final (non-zero) value at the point where the active layer has been fully depleted. Importantly, this saturation value is exactly the charge that survived non-geminate recombination. Upon exciting with a higher fluence, thus increasing the initial amount of charge in the device, the decay of Q_{tot} after a given delay time t_d becomes faster, which is in agreement with higher order non-geminate recombination of free carriers. Upon normalization to the extracted charge at minimum delay, as shown in Figure 2(b), the faster decay with increasing intensity is clearly visible.

As shown before for PTB7:PCBM and other blends, the data can be fit with a fluence- and time-independent bimolecular recombination process. Solid lines represent iterative fits according to Equation (1) (Ref. 21) with $k_2 = 1.6 \times 10^{-11}$ cm^3 s^{-1}. Equation (1) is an iterative scheme to describe the reducing of Q_{tot} with increasing delay due to bimolecular recombination of free charge.

$$Q_{tot}(t + \Delta t) = Q_{coll}(t + \Delta t) + Q_{pre}(t + \Delta t)$$

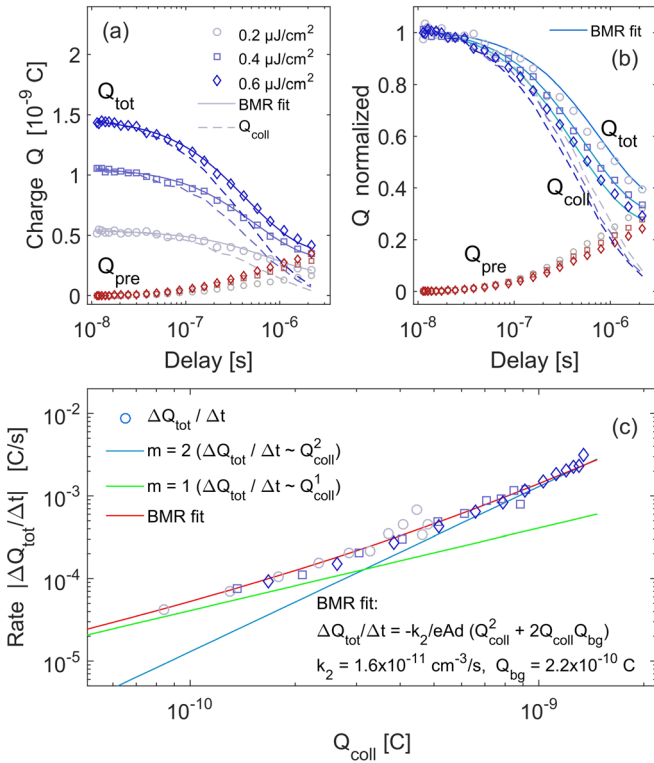$$= Q_{tot}(t) - \frac{k_2}{eAd}\left[Q_{coll}^2(t) + 2Q_{bg}Q_{coll}(t)\right]\Delta t. \quad (1)$$

FIG. 2. (a) Recombination dynamics at $V_{pre} = 0.7$ V for different excitation fluences of the PTB7:PCBM device with a 100 nm active layer thickness and an active area of 1 mm^2. Total extracted charge (Q_{tot}-blue symbols), charge extracted during prebias (Q_{pre}-red symbols), and collected charge (Q_{coll}-dashed lines) vs. delay time, including the iterative fit according to Eq. (1) and (b) normalized extracted charge vs. delay time. (c) Differential extracted charge ($\Delta Q_{tot}/\Delta t$) vs. collected charge (Q_{coll}) for delays starting from 50 ns. The red line represents the fit values according to $\Delta Q/\Delta t = -k_2/(eAd)(Q_{coll}^2 + 2Q_{coll}Q_{bg})$. The fits shown in panels (a)–(c) are computed with the same parameters k_2 and Q_{bg}.

Here, e, A, and d are the elementary charge, device area and active layer thickness, respectively. Note that Eq. (1) also considers recombination of photogenerated free charge with background charge (Q_{bg}), which might have its origin in dark injection or background doping. The main assumption applied here is that the photogenerated charge carriers are distributed equally across the depth of the active layer with the average carrier density $n = Q/eAD$. The very good fit to the data at different fluences and delays verifies the assumption of a fluence- and time-independent recombination coefficient.

To display this important fact in a more illustrative (and convincing) way, the fluence dependent data are re-plotted in a different way which is shown in Figure 2(c). Here, the differential change $\Delta Q_{tot}/\Delta t$ of the total charge is represented as a function of Q_{coll} on a double logarithmic plot. This representation allows to directly read off the apparent recombination order at a given delay time from the slope α according to $\log(\Delta Q_{tot}/\Delta t) \sim \log((Q_{coll})^\alpha) = \alpha \log(Q_{coll})$. For the PTB7: PCBM sample, the differential decay plot can be subdivided into two regimes. For high collected charge (where $Q_{coll} > Q_{bg}$), recombination is mainly between free photogenerated carriers and the data follow a slope $\alpha = 2$ according to $\Delta Q_{tot}/\Delta t = -k_2/(eAd)Q_{coll}^2$. In contrast, if the remaining photogenerated charge is much smaller than the background charge

($Q_{coll} \ll Q_{bg}$), the differential decay is dominated by the recombination with the background charge $\Delta Q_{tot}/\Delta t = -k_2/(eAd)2Q_{bg}Q_{coll}$, which is an effective 1st order process, and $\alpha = 1$. We can exclude that the apparent 1st order recombination dynamics at low carrier densities originate from excitonic recombination as the TDCF method is only sensitive to free charge carriers.

Notably, though this plot collects decay data at different delay times and fluences, all data share the same course. This leads to the important conclusion that the non-geminate recombination loss in this blend is a sole function of the charge present in the layer at t_d, implying a time-independent recombination coefficient. As expected, the entire data set in Figure 2(c) can be satisfactorily described by $\Delta Q_{tot}/\Delta t = k_2/eAd [Q_{coll}(t)^2 + 2Q_{bg}Q_{coll}(t)]$, with the same k_2 as deduced from the iterative fit to the complete data set. The differential decay data in Figure 2(c) are, therefore, fully consistent with exclusive second order recombination in the presence of background charge, with a time-independent recombination coefficient.

The results of TDCF measurements on the planar hybrid perovskite device are summarized in Figure 3. As for the PTB7:PCBM blend, increasing the fluences speeds up recombination, indicative of a higher recombination order. A closer look at the recombination dynamics, however, displays important differences. First, for the planar perovskite device, the initial plateau in the $Q_{tot}(t_d)$ trace is missing. This points to rapid recombination even at a 10 ns scale. Second, $Q_{tot}(t_d)$ approaches the saturation regime already at a delay

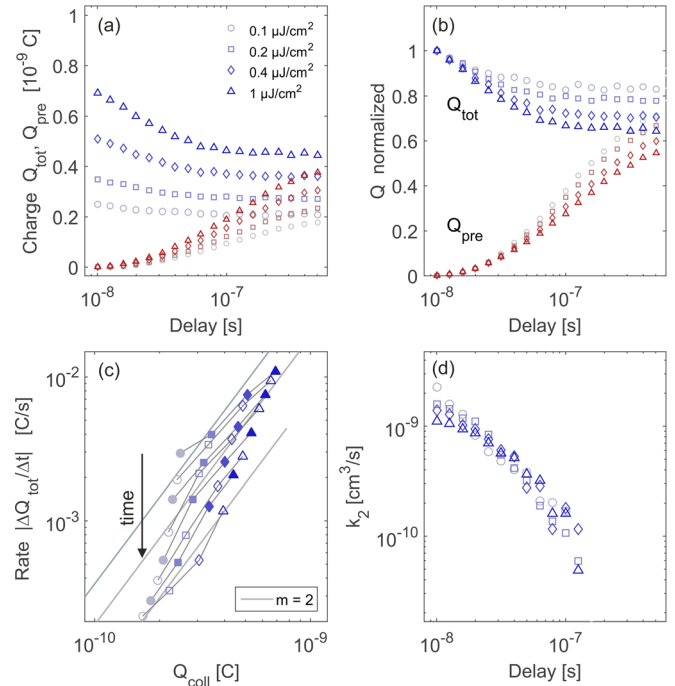FIG. 3. (a) Recombination dynamics for different excitation fluences of the planar perovskite device ($\lambda_{exc} = 532$ nm, $V_{pre} = 0.7$ V). Total extracted charge (Q_{tot}-blue symbols) and charge extracted during prebias (Q_{pre}-red symbols) vs. delay time and (b) normalized extracted charge vs. delay time. (c) Differential extracted charge ($\Delta Q_{tot}/\Delta t$) vs. collected charge (Q_{coll}) for delays from 10 to 60 ns and (d) apparent time-dependent bimolecular recombination coefficients calculated from the data in Figure 3(a) under the assumption of strict bimolecular recombination in the absence of background charge.

time of approx. 100 ns, despite the fact that a significant amount of charge is still present in the layer at this point. This hints to a significant reduction of the recombination rate with increasing delay time and/or decreasing carrier density.

Figure 3(c) shows the same data as in Figure 3(a) in the differential decay plot. Now, in contrast to the all-organic device discussed above, the data do not share one curve. This finding is incompatible with the assumption of a time-independent recombination coefficient, where the recombination rate would be a sole function of the remaining charge carrier density. Interestingly, equitemporal data, measured for a given delay time but with increasing fluence, display a slope of nearly two for all t_d. In other words, for a fixed delay time, the recombination rate follows a second order dependence on charge carrier density, but with a time dependent recombination coefficient. Note that the datapoints in Figure 3(c) do not display a defined transition from an apparent second order to a first order decay with decreasing Q_{coll} (as in Figure 2(c)), meaning that recombination of photogenerated free charge with background charge is insignificant in the planar device for the given illumination and bias conditions. The slope of the equitemporal data is, however, smaller than two for short delay (high fluences), which hints at contributions by an early time first order loss process, e.g., an additional fast surface recombination process or an initial rapid trapping of charges.[13]

Knowing that non-geminate recombination is governed by free carrier recombination (and not affected by background charge), the time-dependent bimolecular recombination coefficients can be calculated from the data in Figure 3(a) to $k_2(t) = -eAd(\Delta Q_{tot}/\Delta t)/Q_{coll}^2$. The result is shown in Figure 3(d) as a function of the delay time. Here, k_2 decreases from an initial value of 10^{-9} cm^3 s^{-1} to below 10^{-10} cm^3 s^{-1} within the first 100 ns, in accordance to a time-dependent bimolecular recombination process. Also, values derived from transients measured at different fluences coincide on the relevant timescale from 10 to 100 ns, meaning that the assumption of a predominant bimolecular recombination process is well justified. Hence, we can certainly interpret the data on the basis of a bimolecular recombination with a time-dependent recombination coefficient.

The data show that recombination at early times after photogeneration is, indeed, very efficient, with k_2 being comparable or even exceeding values deduced from TAS or TRPL experiments on neat perovskite films, but that it experiences a pronounced slow-down when time proceeds. This is in clear contrast to the recombination kinetics of neat perovskite layers as outlined above, which could be consistently explained on the basis of time-independent recombination coefficients.

We have complemented our TDCF studies with TRPL measurements on planar perovskite samples with the organic charge transport layer (PCBM) in varying concentrations. The results shown in the supplementary material[14] reveal a drastic shortening of the PL lifetime when PCBM is coated on top of the active perovskite. This finding is inconsistent with the view of an ideal planar device geometry. With an average perovskite layer thickness of 300 nm and a reported charge diffusion coefficient[15] of $\sim$0.02 cm^2/s, charge extraction times of the order of 10–20 ns are predicted, in clear

contrast to our transient PL results. We presume that the solution-processed PCBM phase interpenetrates the active perovskite material, probably through cracks and grain boundaries. For such a morphology, photogenerated electrons will be rapidly captured by the interpenetrating fullerene network. In agreement with this interpretation, we observe a more rapid PL decay when the perovskite layer is sufficiently covered with PCBM. Likewise, the static PL signal was quenched by a factor of 5. Additionally, we observed a 10 nm blue-shift of the PL peak. This is consistent with the findings that electrons at the trap-rich perovskite surface are quickly captured by the PCBM[27] and only the bulk emission remains.[28]

The significant slow-down of recombination might therefore be caused by the motion of electrons out of the interpenetrating PCBM phase towards the fullerene bulk, thereby reducing the probability of the encounter with holes on the perovskite. In fact, we find that the slow-down of the recombination process is reduced when applying a larger bias closer to V_{oc} (supplementary material). However, a significant power-law dependence of the temporal decay of k_2 is still visible near V_{oc}, pointing to an intrinsic process.

Recent work by Baumann *et al.* revealed the appearance of additional shallow trap states in the PCBM/C$_{60}$ electron transport layer when CH$_3$NH$_3$PbI$_3$ is coated with the latter.[29] These traps might affect the rate of non-geminate recombination. On the other hand values for the bimolecular recombination coefficient in Figure 3(d) at intermediate delay times are still rather high, above 10^{-10} cm^3/s, pointing to a quite weak effect of trapping on the recombination dynamics at the time scale of few tens of nanoseconds.

In summary, the charge carrier recombination dynamics in a working hybrid perovskite solar cell have been measured at excitation densities relevant for device operation, using TDCF. A well-studied organic bulk heterojunction device served as a reference system. In agreement with previous findings[21,22] strict bimolecular recombination applies to explain the observed fluence-dependent recombination dynamics in our prototypical organic bulk heterojunction device. Also, numerical device simulations with a fluence- and time-independent bimolecular recombination coefficient of $k_2 = 1.6 \times 10^{-11}$ cm^3 s^{-1} were fully consistent with experimental current-voltage characteristics of PTB7:PCBM devices at different illumination intensities.[22] In the case of our flat perovskite solar cell, the recombination of extractable charge is also of second order, but now with a time-dependent recombination coefficient. Predominant second order recombination is consistent with lower trap density as reported for planar perovskite layers. TDCF measurements with short delay times reveal an initial bimolecular recombination coefficient of $\sim$10^{-9} cm^3 s^{-1}, comparable to values reported for neat perovskite films. However, the rapid reduction of k_2 within the first tens of nanoseconds results in a vast slowdown of the recombination rate. As a consequence, and in contrast to the organic reference device, free charge recombination in the planar perovskite cell becomes insignificant after ca. 100 ns, despite the fact that mobile charge carriers are still present in the device. We attribute this to the efficient collection of charges generated in the perovskite layer by the two organic charge transport layers within

several nanoseconds. This is consistent with the high power conversion efficiencies demonstrated for those devices. Achieving a complete understanding of the charge carrier recombination dynamics observed with TDCF and its correlation to the device performance will be the subject of further investigations.

[1] W. S. Yang, J. H. Noh, N. J. Jeon, Y. C. Kim, S. Ryu, J. Seo, and S. Il Seok, Science **348**, 1234 (2015).

[2] S. D. Stranks and H. J. Snaith, Nat. Nanotechnol. **10**, 391 (2015).

[3] P. Docampo, J. M. Ball, M. Darwich, G. E. Eperon, and H. J. Snaith, Nat. Commun. **4**, 2761 (2013).

[4] K. Schulze, C. Uhrich, R. Schüppel, K. Leo, M. Pfeiffer, E. Brier, E. Reinold, and P. Bäuerle, Adv. Mater. **18**, 2872 (2006).

[5] D. Bartesaghi, I. del C. Pérez, J. Kniepert, S. Roland, M. Turbiez, D. Neher, and L. J. A. Koster, Nat. Commun. **6**, 7083 (2015).

[6] U. Würfel, D. Neher, A. Spies, and S. Albrecht, Nat. Commun. **6**, 6951 (2015).

[7] C. M. Proctor, M. Kuik, and T.-Q. Nguyen, Prog. Polym. Sci. **38**, 1941 (2013).

[8] T. C. Sum, S. Chen, G. Xing, X. Liu, and B. Wu, Nanotechnology **26**, 342001 (2015).

[9] Y. Yamada, T. Nakamura, M. Endo, A. Wakamiya, and Y. Kanemitsu, J. Am. Chem. Soc. **136**, 11610 (2014).

[10] S. D. Stranks, V. M. Burlakov, T. Leijtens, J. M. Ball, A. Goriely, and H. J. Snaith, Phys. Rev. Appl. **2**, 034007 (2014).

[11] J. S. Manser and P. V. Kamat, Nat. Photonics **8**, 737 (2014).

[12] C. Wehrenfennig, G. E. Eperon, M. B. Johnston, H. J. Snaith, and L. M. Herz, Adv. Mater. **26**, 1584 (2014).

[13] E. M. Hutter, G. E. Eperon, S. D. Stranks, and T. J. Savenije, J. Phys. Chem. Lett. **6**, 3082 (2015).

[14] See supplementary material at http://dx.doi.org/10.1063/1.4944044 for a review of published recombination coefficients, current-voltage characteristics, experimental details, photoluminescence data and AFM images of the planar perovskite film.

[15] S. D. Stranks, G. E. Eperon, G. Grancini, C. Menelaou, M. J. P. Alcocer, T. Leijtens, L. M. Herz, A. Petrozza, and H. J. Snaith, Science **342**, 341 (2013).

[16] G. Xing, N. Mathews, S. S. Lim, Y. M. Lam, S. Mhaisalkar, and T. C. Sum, Science **342**, 344 (2013).

[17] E. Edri, S. Kirmayer, S. Mukhopadhyay, K. Gartsman, G. Hodes, and D. Cahen, Nat. Commun. **5**, 3461 (2014).

[18] C.-H. Chiang, Z.-L. Tseng, and C.-G. Wu, J. Mater. Chem. A **2**, 15897 (2014).

[19] F. X. Xie, D. Zhang, H. Su, X. Ren, K. S. Wong, M. Grätzel, and W. C. Choy, ACS Nano **9**, 639 (2015).

[20] J. Kniepert, M. Schubert, J. C. Blakesley, and D. Neher, J. Phys. Chem. Lett. **2**, 700 (2011).

[21] J. Kniepert, I. Lange, N. J. van der Kaap, L. J. A. Koster, and D. Neher, Adv. Energy Mater. **4**, 1301401 (2014).

[22] J. Kniepert, I. Lange, J. Heidbrink, J. Kurpiers, T. J. K. Brenner, L. J. A. Koster, and D. Neher, J. Phys. Chem. C **119**, 8310 (2015).

[23] Z. He, C. Zhong, S. Su, M. Xu, H. Wu, and Y. Cao, Nat. Photonics **6**, 591 (2012).

[24] F. Deledalle, P. Shakya Tuladhar, J. Nelson, J. R. Durrant, and T. Kirchartz, J. Phys. Chem. C **118**, 8837 (2014).

[25] A. Foertig, J. Kniepert, M. Gluecker, T. Brenner, V. Dyakonov, D. Neher, and C. Deibel, Adv. Funct. Mater. **24**, 1306 (2014).

[26] I. A. Howard, R. Mauer, M. Meister, and F. Laquai, J. Am. Chem. Soc. **132**, 14866 (2010).

[27] Y. Shao, Z. Xiao, C. Bi, Y. Yuan, and J. Huang, Nat. Commun. **5**, 5784 (2014).

[28] Q. Dong, Y. Fang, Y. Shao, P. Mulligan, J. Qiu, L. Cao, and J. Huang, Science **347**, 967 (2015).

[29] A. Baumann, S. Väth, P. Rieder, M. C. Heiber, K. Tvingstedt, and V. Dyakonov, J. Phys. Chem. Lett. **6**, 2350 (2015).